



Effect of bicarbonate on biodegradation behaviour of pure magnesium in a simulated body fluid



Zaichun Li^a, Guang-Ling Song^{b,c,*}, Shizhe Song^a

^a School of Materials Science and Engineering, Tianjin University, Tianjin 300072, China

^b College of Materials, Xiamen University, 422 S Siming Rd, Siming District, Xiamen, Fujian 361005, China

^c The University of Queensland, Materials Engineering, St. Lucia, QLD 4072, Australia

ARTICLE INFO

Article history:

Received 27 September 2013

Received in revised form 17 October 2013

Accepted 20 October 2013

Available online 1 November 2013

Keywords:

Magnesium

EIS

Biodegradability

Surface film

ABSTRACT

The effect of bicarbonate on biodegradation of pure magnesium in a simulated body fluid is investigated by means of X-ray diffraction, X-ray photoelectron spectroscopy, polarization curve and electrochemical impedance spectroscopy. The results show that magnesium biodegrades rapidly and non-uniformly during 27 h of immersion in four simulated body fluid solutions containing different concentrations of bicarbonate. The biodegradation rate first decreases and then increases with time. A small amount of bicarbonate in simulated body fluid has an inhibition effect on the Mg dissolution, while an overdose of bicarbonate addition activates the magnesium surface in the simulated body fluid. The interesting phenomena can be interpreted by a surface film model involving precipitation of calcium carbonate and further ionization of bicarbonate in the simulated body fluids, incorporation of calcium, carbonate and phosphate compounds in the surface film, and development of chloride-induced pitting corrosion damage on the magnesium with time.

© 2013 Elsevier Ltd. All rights reserved.

1. Introduction

New biomaterials normally need to pass in-vitro tests for their biocompatibility before in-vivo experiments. Otherwise, they will not be further considered for possible clinic applications [1]. As most in-vitro tests are conducted in simulated body fluid (SBF) solutions [2–15], SBFs have become important media in development of new biomaterials.

A SBF basically mimics human blood plasma and contains similar levels of the main inorganic components in the human body [16]. In a selected SBF solution, in-vivo behaviours of an implant material can be reproduced or demonstrated to some degree [17]. There have been several SBF solutions with different inorganic ion concentrations developed and used in biocompatibility studies [18–22]. It is important to learn how the inorganic ions in a SBF affect the bioactivity of a biomaterial.

In biomaterial studies, the development of new biodegradable materials is an important topic, because a biodegradable material in the human body can be gradually dissolved, absorbed, consumed and excreted, and thus no secondary surgery is needed to remove it after the surgery region has healed. Magnesium is

potentially a biodegradable material because of its outstanding biological properties [23]. Firstly, Mg²⁺ is an essential element in the human body [24]. It is beneficial to bone strength and growth [25,26]. Secondly, Mg alloys have specific density (1.74–2 g/cm³) and Young's modulus (41–45 GPa) close to those (1.8–2.1 g/cm³, 3–20 GPa) of human body's bones, which make magnesium alloys superior to other artificial implant materials [27]. However, Mg alloys are corroded rapidly in chloride containing solutions [28–33], including the human body fluid or blood plasma [34]. Even worse, the corrosion is always accompanied by hydrogen evolution and solution alkalization [35]. These by-products can delay the healing of surgery region and may even result in necrosis of tissues [36]. To solve the rapid corrosion induced problems, the biodegradation of Mg in the human body must be reliably predicted and effectively controlled. Understanding the in-vitro behaviour of Mg is a key to tailored Mg in-vivo biodegradation, and comprehending the influence of SBF composition on Mg biodegradation performance is a foundation for research aiming at this goal.

There are already many studies investigating the in-vitro and in-vivo biodegradability of Mg alloys [37–42]. Witte et al. [43] compared in-vivo bone responses to four different Mg alloys and found that a higher Mg²⁺ concentration activated bone cells. Song [44,45] proposed a strategy including three basic approaches: (1) purification, (2) alloying and (3) surface treatment/coating to slow down the biodegradation rate of Mg alloys for the human body to gradually adjust, adapt and deal with the hydrogen evolution and solution alkalization. Recently, many more papers [46–55] have

* Corresponding author at: Materials Science and Technology Division, ORNL National Lab, 1 Bethel Valley Rd., PO Box 2008, MS-6159, Oak Ridge, TN 37830, USA. Tel.: +1 248 567 9811; fax: +1 248 567 9811.

E-mail address: guangling.song@gmail.com (G.-L. Song).

Table 1

Ion concentrations (mmol/L) of SBF solutions.

SBF Solution	Na ⁺	K ⁺	Mg ²⁺	Ca ²⁺	Cl ⁻	HCO ₃ ⁻	HPO ₄ ²⁻	SO ₄ ²⁻
Modified SBF-2	117.0	5.0	1.5	2.5	125.0	2.0	1.0	0.5
Modified SBF-15	130.0	5.0	1.5	2.5	125.0	15.0	1.0	0.5
Normal SBF-27	142.0	5.0	1.5	2.5	125.0	27.0	1.0	0.5
Modified SBF-40	155.0	5.0	1.5	2.5	125.0	40.0	1.0	0.5

also been published aiming to improve the biodegradation performance of Mg alloys. However, most of the investigations are mainly focused on understanding the effect of a Mg alloy's composition, microstructure and surface condition on its biodegradability. How the ions in the body fluid affect the corrosion of implanted Mg alloys has rarely been investigated yet [56–58].

This paper investigates the influence of bicarbonate on Mg biodegradation behaviour in a SBF. The selection of bicarbonate as an influencing factor in this study is based on the fact that bicarbonate has a contribution to the composition and structure of calcium phosphates precipitated on a biomaterial [59]. However, its concentration varies in different SBFs [60]. The investigation will help compare and understand the differences in biodegradability when Mg is tested in different SBF solutions. In this regard, there has been an important study [61] showing that the surface film on Mg could become more protective in a SBF when bicarbonate concentration increases from 4 mmol/L to 27 mmol/L. It would be interesting to learn whether the protection performance of the surface film on Mg can be further enhanced if more bicarbonate ions are present in the SBF. A study on the effect of bicarbonate in a wider concentration range on Mg biodegradability will lead to a more comprehensive understanding of the in-vitro and in-vivo biodegradation behaviours of Mg.

2. Experiments

2.1. Sample

1 cm × 1 cm × 1 cm cubic coupons cut from a pure magnesium (99.96 wt%) ingot were used in this study. Some of the coupons abraded with SiC paper (to P#1000), cleaned with distilled water and alcohol and then dried with flowing air were used for immersion test. The other coupons were mounted with epoxy resin and made into electrodes with a 1 cm² area exposed as their working surfaces. The surfaces were also abraded with SiC paper up to P#1000, quickly rinsed with distilled water and alcohol, and then dried in flowing air. All the prepared coupons and electrodes were stored in desiccator before tests.

2.2. Solution

A normal SBF solution (Normal SBF-27) used in this study was prepared using the following analytical chemicals: 6.547 g/L NaCl, 2.268 g/L NaHCO₃, 0.373 g/L KCl, 0.268 g/L Na₂HPO₄·7H₂O, 0.305 g/L MgCl₂·6H₂O, 0.278 g/L CaCl₂, 0.071 g/L Na₂SO₄ and 6.057 g/L (CH₂OH)₂CNH₂ (TRIS). These chemicals were separately dissolved in distilled water to make into concentrated solutions. They were poured into a beaker one by one and continuously stirred. To avoid precipitation, 4 mL of HCl (1 mol/L) was added into the beaker before CaCl₂ addition. After all the chemicals had been fully mixed in the beaker, the solution was diluted with distilled water to a desired volume.

To investigate the effect of bicarbonate on Mg biodegradation behaviour, 3 modified SBF solutions, Modified SBF-2, Modified SBF-15 and Modified SBF-40, were also prepared in the same way as the Normal SBF by simply altering the amount of NaHCO₃ added. The

SBF solutions were adjusted with NaOH to pH 7.4. The inorganic ion concentrations of these SBF solutions are listed in Table 1. The SBF solutions after preparation were used for tests immediately. Their temperatures were controlled at 37 ± 1 °C during tests.

2.3. Tests

The pure Mg coupons were hanged with fine nylon lines and immersed in beakers containing 300 mL of the normal and modified SBF solutions, respectively. After 27 h of immersion, they were taken out and resined with distilled water. Their surface morphologies were observed under a light optical microscope (Olympus BX51M) and recorded with a digital camera.

The corrosion products formed on the Mg surfaces after immersion were analysed by XRD using Rigaku D/Max-2500 X-ray diffraction instrument with Cu K α as X-ray source. Some areas of interest were further investigated by XPS using a PE model PHI-1600 X-ray photoelectron Spectroscopy system.

A traditional three-electrode electrolyte cell was used for electrochemical measurements. The cell contained 300 mL of the SBF solutions, in which the working electrode was the Mg electrode, the counter electrode was a Pt foil, and a Saturated Calomel Electrode (SCE) was used as the reference. All electrochemical tests were conducted using a PARSTAT 2273 electrochemical system.

AC Electrochemical Impedance Spectroscopy (EIS) was employed in this study. EIS spectra were repeatedly measured at the open-circuit potentials at different times after pure Mg had been immersed in the SBF solutions. A 5 mV-amplitude of AC potential perturbation was used to stimulate the Mg/SBF system and the frequency range was set from 100 kHz to 10 mHz. Polarisation curves were measured after the pure magnesium electrode had been immersed in the SBF solutions for 5 min. Potentiodynamic scanning started from -2 V vs. SCE towards an anodic potential at a rate of 15 mV/min until the polarisation current exceeded 100 mA. The EIS and polarization curve measurements were repeated at least 3 times under each condition.

3. Results

3.1. Corrosion morphology

After 27 h of immersion, the Mg specimen surfaces were significantly dissolved. The damage was featured by deposited white corrosion products. The biodegradation of Mg in these SBFs was non-uniform; the damage was distributed in some local areas. Fig. 1 shows some typical areas of the corroded Mg coupons. Apart from the corroded areas covered by white corrosion products, there are some dark or black regions on the specimen surfaces, which appear to be undamaged. The corroded area in Modified SBF-2 is the largest; in Modified SBF-15 the damaged area is smaller; the least corrosion damage appears on the coupon immersed in Normal SBF-27; the damage however becomes more severe again in Modified SBF-40. Based on this observation (Fig. 1), the degrees of corrosion damage or the biodegradation rate of Mg in the four different SBF solutions can be qualitatively rated in the following order:

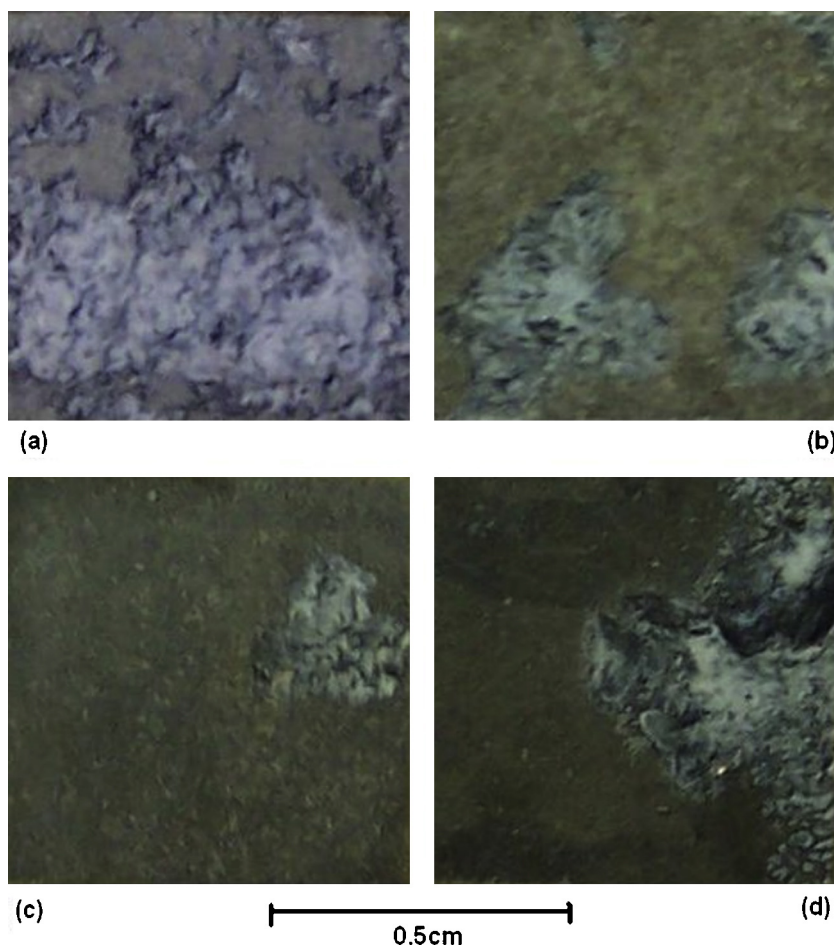


Fig. 1. Surface morphologies of Mg coupons after 27 h of immersion in (a) modified SBF-2, (b) modified SBF-15, (c) normal SBF-27 and (d) modified SBF-40.

Table 2

XPS analysed composition of an “undamaged” surface area for pure magnesium after immersion in normal SBF-27 for 27 h.

Element	O1s	C1s	Mg2p	P2p	Ca2p	Zn2p
Atom. (%)	41.9	41.6	6.1	5.8	4.3	1.4

Modified SBF-2 > Modified SBF-15 > Modified SBF-40 > Normal SBF-27

3.2. Surface composition

The Mg coupon surfaces after 27 h of immersion in the SBF solutions were analysed by XRD. Although the Mg and Mg(OH)₂ peaks in XRD were weak, they can be distinguished from the background noise. Except Mg and Mg(OH)₂, no other signals can be picked up from XRD. Fig. 2 shows a typical XRD spectrum for Mg after immersion in Normal SBF-27.

To more comprehensively learn the surface composition, XPS was utilised to analyse the undamaged surface areas where no white corrosion products were formed. Table 2 lists the composition of such an area on Mg after immersion in Normal-SBF-27 for 27 h. It shows that this area contains some Mg, P, Ca and Zn in addition to large amounts of C and O. As all the SBF solutions contain C, P and Ca, it is not surprising that these elements get onto Mg surfaces after immersion. The Zn signal might be an error of XPS instrument. In this study, the signal intensities of all the elements varied when different spots on Mg were chosen for XPS analysis. This is probably due to the influence by various small amounts of

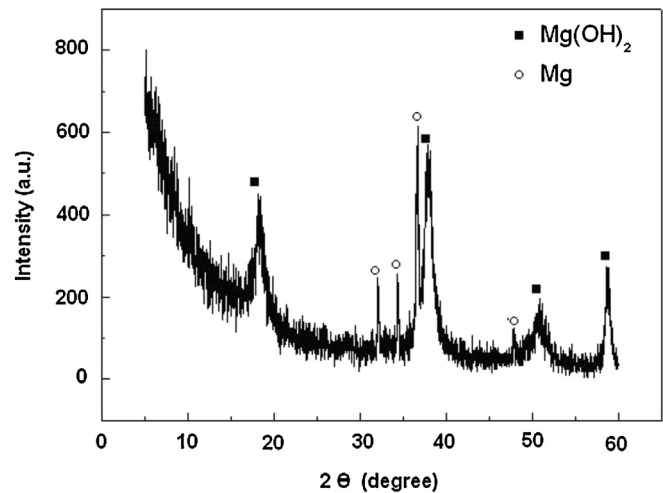


Fig. 2. XRD spectrum for Mg surface after 27 h of immersion in normal SBF-27.

Mg(OH)₂ corrosion products deposited in different areas on the undamaged surface. Hence, it is difficult to quantitatively interpret the XPS results. In this case, a quantitative comparison of the Mg surface compositions after immersion in different SBF solutions is actually meaningless. Nonetheless, a conclusion can still be drawn that the corrosion products on pure Mg immersed in the SBF solutions contain at least P and Ca.

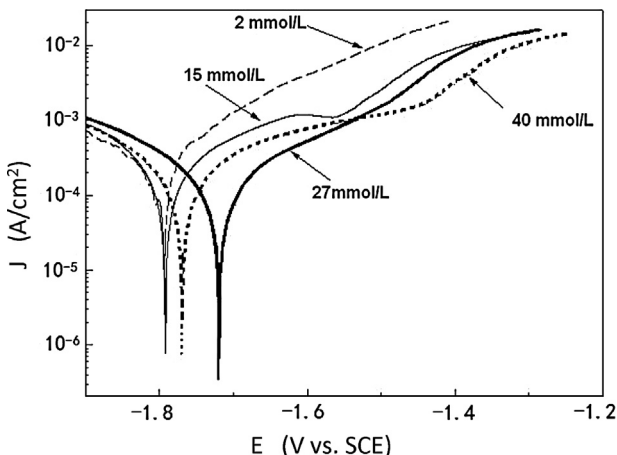


Fig. 3. Polarisation curves of Mg in SBF solutions with different bicarbonate concentrations.

3.3. Polarization curve

The polarization curves of pure Mg in the 4 SBF solutions are presented in Fig. 3. It seems that Mg has similar cathodic polarization curves, but its anodic polarization behaviours are evidently different. There is a wide linear Tafel region on the anodic polarization curve for Mg in Modified SBF-2, but when the bicarbonate concentration becomes higher, the anodic polarization curve

shows two different regions, for example in Modified SBF-15, SBF-27 and SBF-40. It seems that Mg experiences somewhat “passivating” in the relatively low potential range and then becomes “active” in the high potential region in the SBFs containing more than 2 mmol/L bicarbonate. The anodic current densities in the “active” region decrease as more bicarbonate ions are added in the SBF solution. However, the anodic current densities in the “passive” region do not always decrease with increasing bicarbonate concentration; when the SBF contains more than 27 mmol/L of sodium bicarbonate (for example, in SBF-40), the anodic current densities become even higher. For Mg in SBF-15, SBF-27 and SBF-40, the anodic polarization curves in the “passivating” regions have a linear Tafel characteristic.

If the cathodic Tafel regions and anodic Tafel straight lines are extrapolated to the open-circuit potentials, the corrosion rates of Mg in SBF-2, SBF-15, SBF-27 and SBF-40 can be roughly estimated to be 0.25 mA/cm², 0.22 mA/cm², 0.15 mA/cm² and 0.19 mA/cm², respectively. Correspondingly, the corrosivity of these SBF solutions can be rated as follows:

Modified SBF-2 > Modified SBF-15 > Modified SBF-40 > Normal SBF-27 which is the same as the rating based on the corrosion morphologies of the magnesium in these solutions (see Fig. 1).

3.4. AC electrochemical impedance spectrum

The EIS spectra of Mg immersed in the four different SBF solutions are presented in Fig. 4. Generally speaking, they have two

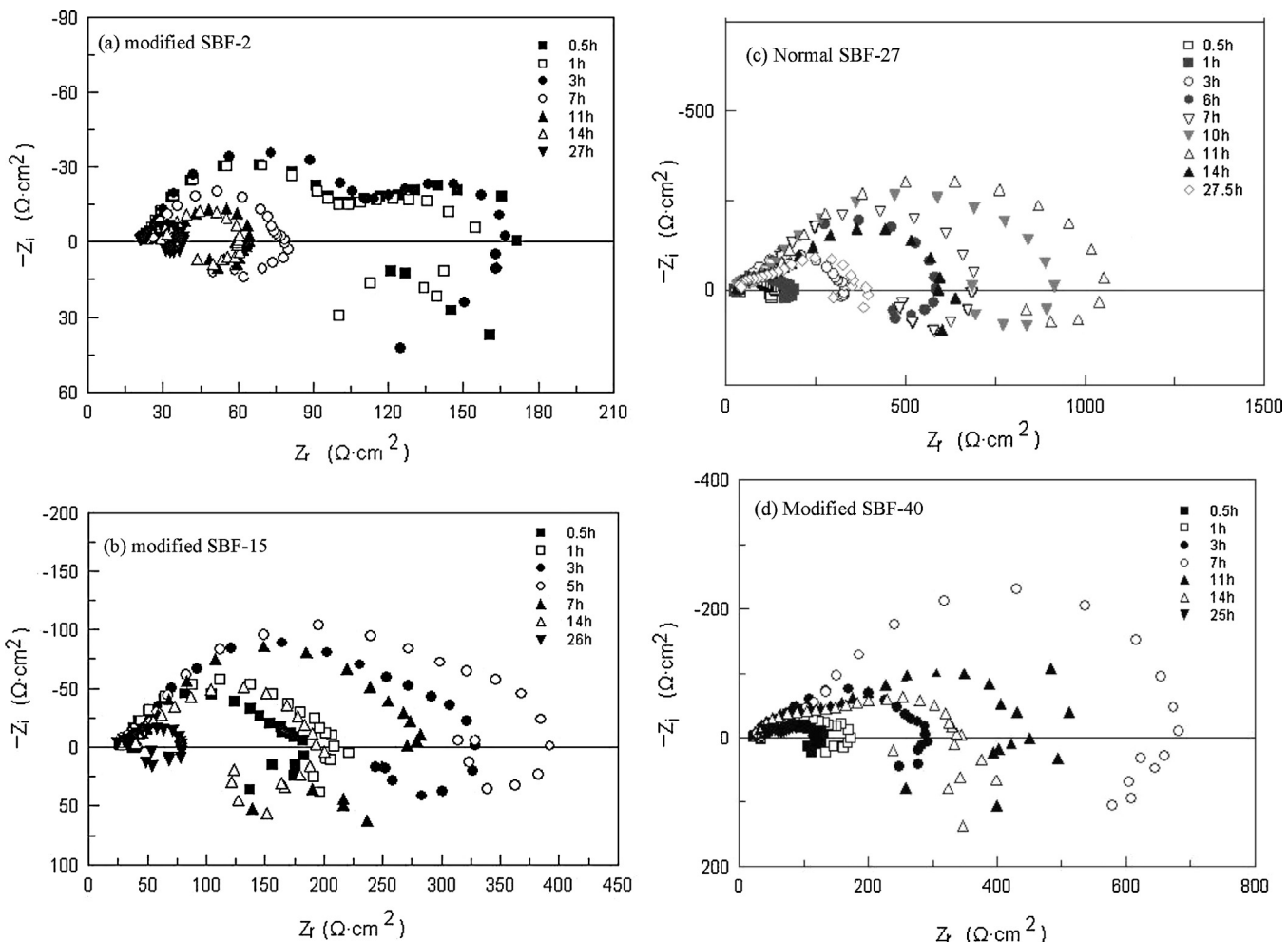


Fig. 4. EISs for Mg measured at different times in different SBF solutions: (a) modified SBF-2, (b) modified SBF-15, (c) normal SBF-27 and (d) modified SBF-40.

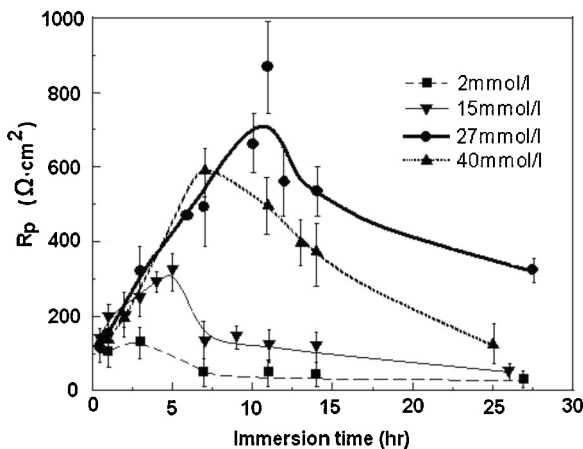


Fig. 5. Polarisation resistance (R_p) estimated from the measured EIS impedance spectra (Fig. 4) for Mg immersed in the SBF solutions.

capacitive loops in the high and mediate frequency ranges and an inductive loop at low frequencies. These impedance features change with immersion time and bicarbonate concentration; some loops become insignificant or disappear.

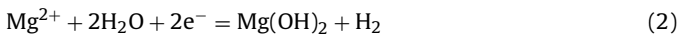
An important result that can be directly obtained from an EIS spectrum is polarisation resistance R_p , which measures the distance from the highest frequency point (in theory frequency $\rightarrow \infty$) to the lowest frequency point (theoretically frequency $\rightarrow 0$) on axis (Z_r) of the real part of impedance. Fig. 5 summarises the R_p values estimated from the measured EISs (Fig. 4). It is found that R_p first increases and then decreases with immersion time. Both the maximum R_p value and the corresponding time increase while bicarbonate concentration is increasing from 2 mmol/L to 27 mmol/L, and then decrease when bicarbonate concentration further increases to 40 mmol/L.

The variation of EIS characteristics and the dependence of R_p on bicarbonate concentration as shown Figs. 4 and 5 are in good agreement with the influences of bicarbonate on corrosion damage morphology (Fig. 1) and polarization curve (Fig. 3), suggesting that a complicated surface film mechanism might be involved in the biodegradation process of pure Mg in the SBF solutions.

4. Discussion

4.1. The biodegrading surface

It is well known that Mg can be dissolved in an aqueous solution through reactions [35]:



The main corrosion product formed on a corroded Mg surface is Mg(OH)_2 . Even in an atmospheric environment, the surface film also consists of Mg(OH)_2 mixed with some MgO [44,62,63]. Therefore, Mg(OH)_2 will be undoubtedly a major component of the corrosion product film formed in an aqueous SBF solution. The XRD (see Fig. 2) in this study confirms this. The Mg(OH)_2 peaks should mainly come from corroded areas, where the corrosion product layer is relatively thick and detectable by XRD. However, due to the low sensitivity of XRD to element concentration, the presence of other elements in the corroded area cannot be excluded, but if any their amounts should be negligible compared with Mg(OH)_2 .

Elements P and Ca detected by XPS (Table 2) in this study is in agreement with the results reported in literature [43] which shows that significant amounts of P and Ca measured in the

corrosion products after magnesium rods were implanted in guinea pigs for a few weeks, and the P-Ca product was identified as calcium phosphate [43]. In fact, SBF is a solution highly supersaturated with respect to a Ca and P containing apatite [64]. Since Mg can promote the precipitation of calcium phosphate in an in-vitro environment [65,66], the precipitation of Ca and P containing compounds on Mg surface together with Mg(OH)_2 is a very reasonable result in this study.

The Mg(OH)_2 containing film should have been formed on Mg in SBF solutions before corrosion damage occurs. For example, Xin et al. [61] clearly show an undamaged Mg surface covered by a corrosion product film after 24 h of immersion in a SBF. Thus, the undamaged area in this paper does not mean no surface film formed; it simply refers to a region where corrosion is not so severe and thus invisible by naked eye. The XPS results (see Table 2) of the undamaged area indicate that C, P and Ca are mixed in a Mg(OH)_2 film. In fact, surface film containing C, P and Ca elements on a Mg-RE alloy in a SBF has been reported [67]. Other researchers [68] have also detected carbonates and phosphates on Mg in SBFs. Yamamoto and Hiromoto [69] found that the surface layers (mainly Mg(OH)_2) on pure Mg in Earle and MEM fluids also contain Mg, O, Ca, P and C, and their concentrations are even close to the element contents measured in this study.

The composition of the corrosion product film or surface film on Mg in SBF may be interpreted according to the solubilities of Mg and Ca compounds [70]. $\text{Mg}_3(\text{PO}_4)_2$ is almost insoluble in water (lower than 0.0034 mmol/L), and the solubility of $\text{Ca}_3(\text{PO}_4)_2$ is as low as 0.0038 mmol/L. Precipitation of the supersaturated $\text{Mg}_3(\text{PO}_4)_2$ and $\text{Ca}_3(\text{PO}_4)_2$ from the SBFs on Mg after immersion should be expectable. Hence, the measured element Ca on Mg should correspond to $\text{Ca}_3(\text{PO}_4)_2$, and the element P should come from $\text{Mg}_3(\text{PO}_4)_2$ and $\text{Ca}_3(\text{PO}_4)_2$ (see Table 2). Moreover, the solubilities of CaCO_3 and Mg(OH)_2 are 0.067 mmol/L and 0.12 mmol/L, respectively, which are also relatively low compared with other compounds. These two compounds can also reasonably precipitate on Mg if triggered by solution alkalization resulting from Mg dissolution. The most unlikely deposited compounds are MgCO_3 and Ca(OH)_2 , as they have a relatively high solubility (~21 mmol/L). Although chemical reactions have been proposed for precipitation of MgCO_3 a Mg alloy in SBFs [61], this compound is actually not often detected on Mg under an immersion conditions. The other ions, such as K^+ , Na^+ , Cl^- and SO_4^{2-} , are highly soluble and their contributions to the surface film composition in theory should be negligible.

The above explanation based on compound solubilities is only applicable to an undamaged Mg surface in the initial stage of immersion. In the later stage on a corroded surface, the large quantity of corrosion product Mg(OH)_2 will overwhelm the signals of relatively small amounts of $\text{Mg}_3(\text{PO}_4)_2$, $\text{Ca}_3(\text{PO}_4)_2$ and CaCO_3 precipitates. Hence only Mg(OH)_2 is detected by XRD (see Fig. 2).

According to the XRD (Fig. 2) and XPS (Table 2) results and the compound solubility analysis, a conclusion can be drawn that the corroded Mg surface is mainly covered by Mg corrosion product Mg(OH)_2 , while on the undamaged area Mg(OH)_2 , $\text{Mg}_3(\text{PO}_4)_2$, $\text{Ca}_3(\text{PO}_4)_2$ and CaCO_3 are important components of the surface film. Fig. 6(a) schematically illustrates the surface film on Mg in a SBF.

4.2. Effect of bicarbonate

It has been reported [61] that the addition of bicarbonate can reduce the biodegradation damage of Mg in SBF when the bicarbonate concentration is not higher than 27 mmol/L. However, no theoretical explanation has been proposed for this experimental result. The current study confirms this inhibition effect of bicarbonate (Figs. 1, 3 and 5). More interestingly, it shows that bicarbonate in the SBF at a higher concentration, for example at 40 mmol/L,

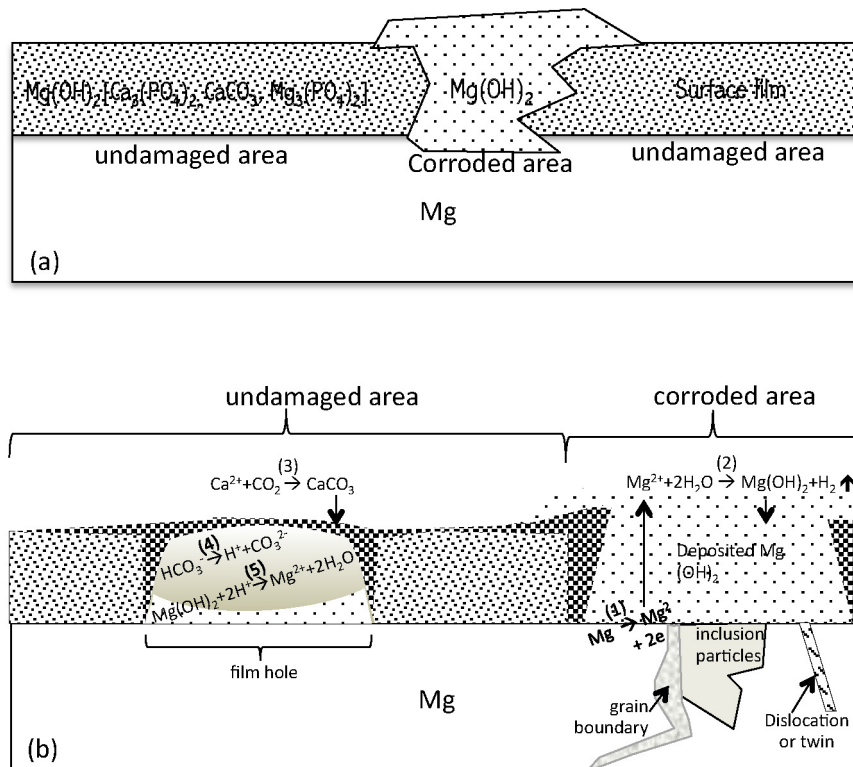


Fig. 6. Surface film models for Mg in normal and modified SBF solutions: (a) the composition model for the surface films formed in the undamaged and corroded areas, (b) the simplified surface film model for reactions involved in the undamaged and corroded areas.

can actually activate Mg surface. This is a new finding. The surface film model proposed above (Fig. 6) may provide a basis for understanding this complicated influence of bicarbonate on the Mg biodegradation performance.

The influence of carbonate concentration on the polarization behaviour of Mg (see Fig. 3) can be related to the variation of Mg surface state in SBF. The “active” and “passivating” regions on the polarization curves should correspond to corroded and undamaged surface states, respectively, of Mg in the SBFs. Chloride can attack a metal, and the attack becomes more aggressive at a higher polarization potential, leading to a sudden increase in anodic current density if the potential exceeds a critical point. When the chloride attack occurs on Mg, the breakdown of surface film in some local areas should be responsible for the dramatically increased anodic current densities [71].

In this study, the anodic current densities in the “active” region suppressed by bicarbonate addition (Fig. 3) can be attributed to the inhibition effect of bicarbonate on Mg. It has been reported that in a chloride containing solution, a small amount of NaHCO_3 can effectively retard the dissolution of Mg, because the added bicarbonates can repel the chlorides adsorbed on Mg surface [72]. This $\text{Cl}^-/\text{HCO}_3^-$ competition mechanism can also explain the inhibition effect of bicarbonate on the “active” behaviour of Mg in SBF (see Fig. 3). The breakdown of surface film could initiate from a defect point where is most easily attacked by chlorides and also preferentially adsorbed by carbonates. The addition of more bicarbonate ions will enhance the competitiveness of HCO_3^- against Cl^- , delay the chloride attack, and thus suppress the “active” current densities.

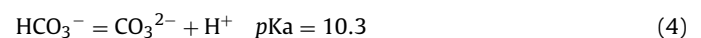
It is more important to understand the effect of bicarbonate on “passivating” behaviour of Mg in the SBFs (see Fig. 3), as the polarization behaviour around the open-circuit potential is closely associated with the Mg biodegradation performance. When bicarbonate concentration has not exceeded 27 mmol/L, the increasing “passivating” tendency with bicarbonate concentration can be

attributed to more CaCO_3 precipitated and incorporated in the surface film on Mg. An increase in bicarbonate concentration should facilitate the following reaction:



This reaction is favoured at a high pH value. According to $\text{Mg}(\text{OH})_2$ solubility (0.12 mmol/L) and solubility product constant (5.61×10^{-12}) [70], the pH value of a $\text{Mg}(\text{OH})_2$ saturated solution should be ~ 11.3 , and a very small amount of $\text{Mg}(\text{OH})_2$ dissolved will result in a solution saturated by $\text{Mg}(\text{OH})_2$ having a pH value 11. It has been measured that an acidic solution quickly becomes basic and its pH value approaches 11 in a few minutes after Mg alloys are immersed in the solution [73]. The solution alkalization can result in more CaCO_3 precipitated together with $\text{Mg}_3(\text{PO}_4)_2$ and $\text{Ca}_3(\text{PO}_4)_2$ to the $\text{Mg}(\text{OH})_2$ surface film on Mg, which further increases the film compactness, improves the polarization resistance of Mg in SBF, and suppresses the anodic current densities in the “passivating” range on the polarization curve (see Fig. 3).

However, if an overdose of HCO_3^- is added, after all the Ca^{2+} cations in BSF deposit through reaction (3), the excess bicarbonates cannot further facilitate CaCO_3 deposition or increase the “passivating” tendency of Mg. Instead, the additional bicarbonates may have a detrimental effect on Mg surface film. In this study, when the content of bicarbonate in SBF increases from 27 mmol/L to 40 mmol/L, the anodic current densities in the “passivating” region become higher (see Fig. 3). This “abnormal” behaviour may be caused by ionization of the excess bicarbonates and dissolution of $\text{Mg}(\text{OH})_2$ by the released protons from the excess bicarbonates:



The acidity point ($p\text{K}_a$) of HCO_3^- is 10.3 [70]. The establishment of equilibrium reaction (4) tends to maintain the solution at pH

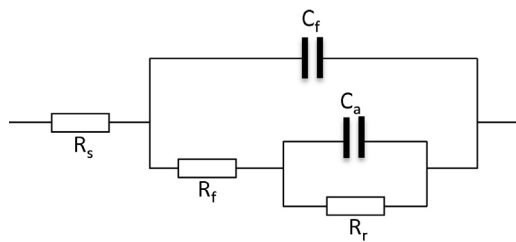


Fig. 7. Equivalent circuit for Mg in the SBF solutions.

values around 10.3, which will retard the solution alkalization to the $\text{Mg}(\text{OH})_2$ saturation pH value ($\text{pH} \sim 11.3$). Consequently, the addition of an overdose of HCO_3^- in SBF will facilitate the dissolution of $\text{Mg}(\text{OH})_2$ film through reaction (5), decrease the film thinner (or increase the film porosity), activate the Mg surface and eventually increase the anodic current densities in the “passivating” region (Fig. 3).

It should be noted that the surface film model (Fig. 6(a)) simply describes the overall surface film composition. To gain a deeper insight into the microstructure and of the surface film its evolution with time on Mg in SBF, a comprehensive EIS analysis is needed.

4.3. Surface film evolution

To better understand the EIS results (Figs. 4 and 5), the surface film model (Fig. 6(a)) should be simplified. The corroded Mg surface can be represented by a film-free area that contains various defects, such as impurity particle, grain boundary, dislocation and twin. This area is preferentially attacked by chlorides and the corrosion damage spreads out from there with time. The surface film on the undamaged area is actually porous. This is understandable, because the surface films on Mg alloys in chloride-containing solutions are generally believed to be porous. The high anodic current densities in the “passivating” regions (Fig. 3) also suggest a porous film on Mg in the SBFs. These micro-pores can be simplified into a hole in the film on the undamaged Mg surface. Therefore, a simplified model can be schematically illustrated as a surface film with a hole and a film-free corroding surface area (see Fig. 6(b)). Such a porous surface film should have an equivalent circuit as shown in Fig. 7, which will be further discussed later.

From AC electrochemical impedance spectra (EISs) (Fig. 4), the estimated R_p results (Fig. 5) suggest that the biodegradation of magnesium in the SBF solutions slows down in the first a few hours and then speeds up again. This behaviour can be ascribed to the evolution of the Mg surface film in composition and microstructure with immersion time. The R_p estimated from an EIS spectrum actually represents an overall corrosion resistance. It is determined by the composition and microstructure of the surface film, and can normally be characterized by a few electrochemical parameters. These characteristic parameters can be obtained through curve-fitting of the capacitive semicircles in the high and mediate frequency ranges of a measured EIS spectrum.

It has been reported [63] that the capacitive loop at high frequencies is a direct response of the surface film on Mg to AC potential stimulation; the relatively low frequency capacitive loop is related to an electrochemical reaction of Mg in a film-free area (corroding area); the inductive loop represents an auto-catalytic damage process of the surface film. As an auto-catalytic reaction cannot be a stable process, the corresponding inductive data points at low frequencies are scattered and difficult to compare for Mg in different SBFs. To simplify the theoretical analysis, the low frequency inductive points are ignored in EIS curve-fitting in this study. This will not significantly affect the extraction of other more useful parameters from the EIS spectra.

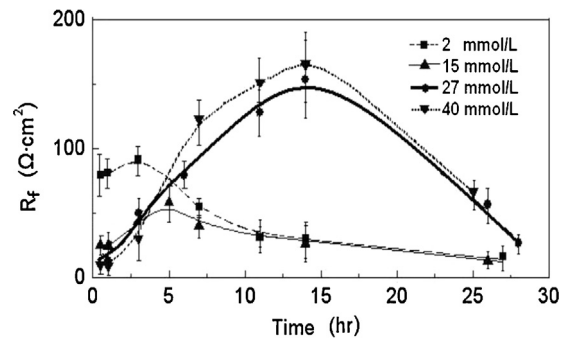


Fig. 8. Surface film resistance (R_f) estimated from the high frequency capacitive loops of the measured EISs (Fig. 4) for Mg in the SBF solutions.

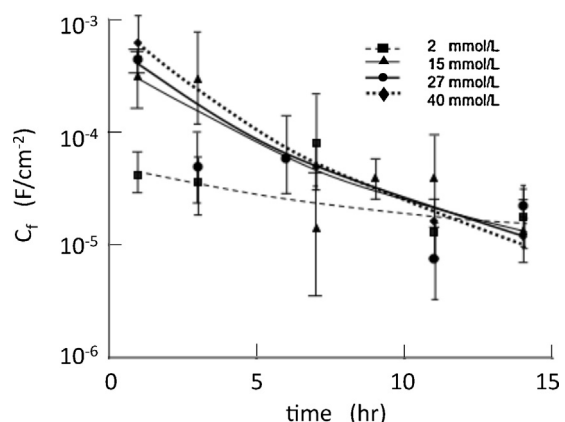


Fig. 9. Film capacitance (C_f) estimated from the high frequency capacitive loops of the measured EISs (Fig. 4) for Mg in the SBF solutions.

To extract the electrochemical parameters, an equivalent circuit as shown in Fig. 7 is adopted. This is a typical equivalent circuit modelling a porous film on an electrode and has been successfully used for Mg surface films [74] and recently in characterizing the degradation behaviour of Mg in SBFs with different concentrations of HCO_3^- [61]. In this equivalent circuit, R_s represents the SBF solution resistance between Mg and reference electrode; R_f is the resistance of surface film on Mg, which in theory is a charge transfer resistance, and its value depends on the compactness or porosity of the film and can also be affected by conductivity of the solution in film pores; C_f stands for the capacitance of the surface film, which is determined by the film thickness and porosity (or roughness); R_r denotes the electrochemical reaction resistance of Mg with water in film pores, which can be retarded by precipitates at the pore bottom; C_a symbolizes a pseudos capacitance resulting from the response of the Mg electrochemical process to AC potential perturbation in the film pores.

The values of the film resistance (R_f), film capacitance (C_f), and electrochemical reaction resistance (R_r) of Mg in film pores estimated from the measured EISs (Fig. 4) through curve-fitting using the equivalent circuit (Fig. 7) are plotted in Figs. 8–10, respectively. As C_a has very scattered points and its physical meaning is not as clear as the other parameters, it is not presented and discussed in this paper. Figs. 8 and 10 show that R_f and R_r increase first and then decrease with time, and share a similar evolution trend with R_p (Fig. 5), having a maximum during immersion. The maximum R_f , R_r and R_p phenomena could result from a combination of the improving overall surface film stability and the increasing pitting susceptibility of Mg with immersion time.

Before immersion, the initial Mg surface film formed in air mainly consists of $\text{Mg}(\text{OH})_2$ mixed with some MgO [62] and does

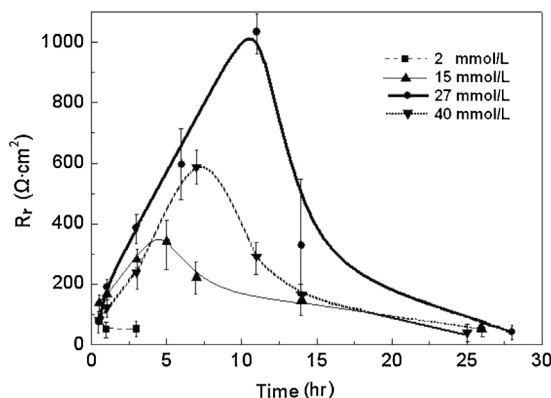


Fig. 10. Electrochemical reaction resistance (R_r) of Mg in film pores estimated from the low frequency capacitive loops of the measured EISs (Fig. 4) for Mg in the SBF solutions.

not have a significantly corroded area. After immersion starts, because of the reactions of Mg and MgO with water, the pH value of BSF gradually increases and MgO is converted to $Mg(OH)_2$. In the increasingly alkalinized SBF, $Mg_3(PO_4)_2$, $Ca_3(PO_4)_2$ and $CaCO_3$ start to precipitate and are gradually incorporated into the surface film. Thus, the surface film becomes more stable with time. The precipitation of $Mg_3(PO_4)_2$ should be more likely to occur in the film pores, where Mg^{2+} concentration is higher, while $Ca_3(PO_4)_2$ and $CaCO_3$ should be mainly distributed outside film pores or over the pore "mouths" where there are sufficient Ca^{2+} cations. Although the migration of Ca^{2+} cations into film pores could be slower than Cl^- , HCO_3^- and HPO_4^{2-} anions, a small amount of Ca^{2+} may still diffuse into film pores and precipitate in a small amount at the pore bottom after reaction with carbonate and phosphate anions there. As a result, the precipitation of $Ca_3(PO_4)_2$ and $CaCO_3$ in large amounts around the pore "mouths" will narrow the pores and even close the pore "mouths"; the precipitation of some $Mg_3(PO_4)_2$ and a very limited amount of $CaCO_3$ in the film pores at their bottoms will retard the electrochemical reaction of Mg. Therefore, according to the surface film model (Fig. 6), both R_f and R_r increase with immersion time (Figs. 8 and 10).

It should be noted that the chloride in SBFs is always a corrosive species that can attack Mg particularly at its defect points. In the early stage of immersion, due to relatively large amounts of HCO_3^- and HPO_4^{2-} present in SBF acting as inhibitors protecting Mg, no significant localized corrosion damage occurs. However, after a certain period of immersion time, the HCO_3^- and HPO_4^{2-} anions in SBF should have been consumed by deposition, there will be no sufficient HCO_3^- and HPO_4^{2-} anions in SBF to repel Cl^- ions from Mg surface. For example, Song [44] demonstrated that the consumption of phosphate in a SBF solution led to an increased dissolution rate of Mg. Hence, the consumption of inhibitive HCO_3^- and HPO_4^{2-} anions through precipitation reactions in the later stage of immersion makes Mg more susceptible to corrosion attack especially at defect points. In this case, corrosion will initiate at a defect point, for example in a relatively large film pore where the substrate Mg happens to have an impurity inclusion or crystallographic defect (such as grain boundary, twin, or dislocation), and then spread out with time from that defect area. In the corroded area, due to the rapid dissolution of Mg, a thick loose $Mg(OH)_2$ layer may be deposited there. This loose corrosion product cannot effectively protect the substrate Mg. Thus, the overall film resistance and the Mg electrochemical reaction resistance in this area will be extremely low. According to the surface film model (Fig. 6(b)) and equivalent circuit (Fig. 7), R_f and R_r will become smaller with time (Figs. 8 and 10).

Either the reduction of film porosity in the undamaged area or the formation of a thick loose $Mg(OH)_2$ corrosion product

layer in the corroded area can lead to a decrease in film capacitance. Thereby, C_f decreases with immersion time (Fig. 9). These C_f results also further support the proposed surface film model (Fig. 6).

With the surface film model (Fig. 6), the influences of bicarbonate concentration on R_f and R_r (Figs. 8 and 10) can also be understood. At the beginning of immersion, before a significant amount of $CaCO_3$ starts to precipitate, an increase in bicarbonate concentration in SBF will result in more bicarbonates getting into the film pores, which increases the solution conductivity in the film pores. Consequently, R_f decreases with increasing concentration of bicarbonate when Mg is first immersed in SBF (Fig. 8). With immersion time, due to Mg dissolution and solution alkalization, more bicarbonate ions added in SBF can cause more $CaCO_3$ precipitated (reaction (3)) on Mg to close the film pore "mouths". Thereby, R_f increases to a higher value until local damage of the film caused by chlorides. This explains the maximum R_f value increases as more bicarbonate ions are added into SBF (Fig. 8).

The addition of bicarbonate anions cannot immediately influence the Mg electrochemical reaction at the bottom of a film pore. That is why R_r does not vary significantly with bicarbonate concentration at the beginning of immersion (Fig. 10). However, as immersion continues and solution alkalizes, addition of more bicarbonate anions can lead to more $CaCO_3$ precipitated at the bottoms of film pores, which can effectively stop or at least slow down the electrochemical reaction of Mg from the pore bottoms. Hence, R_r increases with increasing bicarbonate concentration. However, the precipitation of $CaCO_3$ in film pores is limited by the amount of Ca^{2+} . When a too large amount of HCO_3^- is added in SBF, while there are not enough Ca^{2+} ions in the film pores to react with HCO_3^- to form $CaCO_3$ precipitation, the excess HCO_3^- ions could actually retard the alkalization of the pore solution, because the acidity point pK_a of bicarbonate is lower than the pH value of a $Mg(OH)_2$ saturated solution [70]. This acidifying effect of the excess bicarbonates is beneficial to the electrochemical reaction of Mg at the pore bottoms. Therefore, if the bicarbonate concentration is too high in SBF, R_r decreases. This should be the case for Mg in SBF when the concentration of bicarbonate increases from 27 mmol/L to 40 mmol/L (Fig. 10).

Due to the scattered data points, Fig. 9 does not show a clear increase in C_f with bicarbonate concentration in the later stage of immersion. However, the relatively lower C_f value at 2 mmol/L than those at higher concentrations in the initial stage of immersion suggests that the increasing bicarbonate concentration may facilitate the dissolution of the $Mg(OH)_2$ surface film, leading to an increased C_f before significant alkalization of solution occurs. This C_f behaviour is also consistent with the initial R_f results (Fig. 8).

The dependence of R_p (Fig. 5) on bicarbonate concentration similar to that of R_r (Fig. 10) implies that R_r has a bigger contribution than R_f to R_p . This can also be supported by the much larger values of R_r (Fig. 10) than R_f (Fig. 8). It means that the surface film formed on Mg in SBF is very porous and cannot offer sufficient protection for Mg.

The phenomenon that R_r and R_p first increase and then decrease with immersion time has not been reported before. Under similar conditions, Xin et al. [61] only found that the impedance of Mg in their SBFs continuously increased with immersion time. A possible factor responsible for the different EIS results is probably the low Cl^- concentration in their SBFs; This makes their SBFs not aggressive enough to initiate the localized corrosion on Mg in 1-day immersion test, and therefore the maximum R_r and R_p were postponed and missed by their EIS measurements. This will be verified in a more comprehensive investigation on interaction of inorganic ions (including Cl^-) in SBF. The effects of all those ions on Mg biodegradation behaviour will be reported in a separated paper soon.

5. Conclusions

- 1) The biodegradation of Mg in the SBF solutions is a rapid non-uniform process. This signifies that a limited amount of Mg dissolved may lead to severe damage in a local area and result in a premature failure of a Mg implant component.
- 2) The biodegradation rate of Mg in the SBF solutions decreases in the first few hours and then increases with time. This interesting process has not been reported before. The complicated in-vitro biodegradation behaviour of Mg suggests that the biodegradation of Mg may not always slow down with time; the process may be accelerated some time.
- 3) The minimum biodegradation rate of Mg during immersion probably results from a combination of the improvement of overall surface film stability by precipitated calcium, carbonate and phosphate compounds and the development of localized corrosion damage of Mg by chlorides.
- 4) Another new finding is that a small amount of bicarbonate in SBF improves the corrosion resistance of the surface film on Mg, but the biodegradation performance of Mg deteriorates when SBF contains a too high concentration of bicarbonate. Precipitation of CaCO_3 and ionization of HCO_3^- at low and high bicarbonate concentrations respectively should be responsible for this interesting effect of bicarbonate on Mg biodegradation in SBF.
- 5) Since a few hour immersion in a SBF solution can improve Mg corrosion resistance, to avoid the early-stage rapid dissolution of Mg after implantation, in future we can consider soaking a Mg implant in a SBF to form a stable surface film before surgery. This should significantly reduce Mg initial activity, simplify its corrosion process, and make the biodegradation behaviour of an implanted Mg predictable in practice.

References

- [1] LL. Hench, *Bioceramics: from concept to clinic*, *J. Am. Ceram. Soc.* 74 (1991) 1487–1510.
- [2] S. Virtanen, I. Milosev, E. Gomez-Barrena, R. Trebse, J. Salo, Y.T. Konttinen, Special modes of corrosion under physiological and simulated physiological conditions, *Acta Biomater.* 4 (2008) 468–476.
- [3] C. Delgado-Alvarado, P.A. Sundaram, Corrosion evaluation of Ti-48Al-2Cr-2Nb (at%) in Ringer's solution, *Acta Biomater.* 2 (2006) 701–708.
- [4] K. Yu, L. Chen, J. Zhao, S. Li, Y. Dai, Q. Huang, Z. Yu, In vitro corrosion behavior and in vivo biodegradation of biomedical b-Ca₃(PO₄)₂/Mg-Zn composites, *Acta Biomater.* 8 (2012) 2845–2855.
- [5] L. Jonasova, F.A. Muller, A. Helebrant, J. Strnad, P. Greil, Hydroxyapatite formation on alkali treated titanium with different content of Na⁺ in the surface layer, *Biomaterials* 23 (2002) 3095–3101.
- [6] L. Jonasova, F.A. Muller, A. Helebrant, J. Strnad, P. Greil, Biomimetic apatite formation on chemically treated titanium, *Biomaterials* 25 (2004) 1187–1194.
- [7] F. Barrere, C.A. van Blitterswijk, K. de Groot, P. Layrolle, Influence of ionic strength and carbonate on the Ca-P coating formation from SBFx5 solution, *Biomaterials* 23 (2002) 1921–1930.
- [8] F. Barrere, C.A. van Blitterswijk, K. de Groot, P. Layrolle, Nucleation of biomimetic Ca-P coatings on Ti6Al4V from a SBFx5 solution: influence of magnesium, *Biomaterials* 23 (2002) 1921–1930.
- [9] P. Li, C. Ohtsuki, T. Kokubo, Apatite formation induced by silica gel in a simulated body fluid, *J. Am. Ceram. Soc.* 75 (1992) 2094–2097.
- [10] P. Li, X. Te, J. Kangasniemi, J. de Blieck-Hogervorst, C. Klein, K. de Groot, In vivo calcium phosphate formation induced by sol-gel-prepared silica, *J. Biomed. Mater. Res.* 29 (1995) 325–328.
- [11] W. Zhou, T. Shen, N.N. Aung, Effect of heat treatment on corrosion behaviour of magnesium alloy AZ91D in simulated body fluid, *Corros. Sci.* 52 (2010) 1035–1041.
- [12] M. Jamesh, S. Kumar, T.S.N.S. Narayanan, Corrosion behavior of commercially pure Mg and ZM21 Mg alloy in Ringer's solution-long term evaluation by EIS, *Corros. Sci.* 53 (2011) 645–654.
- [13] G. Han, J.-Y. Lee, Y. Kim, J.H. Park, D. Kim, H. Han, S. Yang, H. Seok, Preferred crystallographic pitting corrosion of pure magnesium in Hanks' solution, *Corros. Sci.* 63 (2012) 316–322.
- [14] G. Wu, Y. Zhao, X. Zhang, J.M. Ibrahim, P.K. Chu, Self-protection against corrosion of aged magnesium alloy in simulated physiological environment, *Corros. Sci.* 68 (2013) 279–285.
- [15] T.M. Manhabosco, S.M. Tamborim, C.B. Dos Santos, I.L. Muller, Tribological electrochemical and tribo-electrochemical characterization of bare and nitride Ti6Al4V in simulated body fluid solution, *Corros. Sci.* 53 (2011) 1786–1793.
- [16] T. Kokubo, Bioactive glass ceramics: properties and applications, *Biomaterials* 12 (1991) 155–163.
- [17] T. Kokubo, H. Kushitani, S. Sakka, T. Kitsugu, T. Yamauro, Solutions able to reproduce in-vivo surface structure changes in bioactive A-W glass-ceramics, *J. Biomed. Mater. Res.* 24 (1990) 721–734.
- [18] M.R. Filgueiras, G.L. Torre, L.L. Hench, Solution effects on the surface reactions of a bioactive glass, *J. Biomed. Mater. Res.* 27 (1993) 445–453.
- [19] C. Ohtsuki, H. Kushitani, T. Kokubo, S. Kotani, T. Yamamuro, Apatite formation on the surface of ceratival-type glass-ceramic in the body, *J. Biomed. Mater. Res.* 25 (1991) 1363–1370.
- [20] A. Oyane, H.M. Kim, T. Furuya, T. Kokubo, T. Miyazaki, T. Nakamura, Preparation and assessment of revised simulated body fluids, *J. Biomed. Mater. Res.* 65 (2003) A:188–A:195.
- [21] A. Oyane, K. Onuma, A. Ito, H.M. Kim, T. Kokubo, T. Nakamura, Formation and growth of clusters in conventional and new kinds of simulated body fluids, *J. Biomed. Mater. Res.* 64 (2003) A:339–A:348.
- [22] H. Takadama, M. Hashimoto, M. Mizuno, T. Kokubo, Round-robin test of SBF for in vitro measurement of apatite-forming ability of synthetic materials, *Phosphorus Res. Bull.* 17 (2004) 119–125.
- [23] H.G. Seiler, H. Sigel (Eds.), *Handbook on Toxicity of Inorganic Compounds*, Marcel Dekker Inc, NY, USA, 1988.
- [24] J. Vormann, Magnesium: nutrition and metabolism, *Mol. Aspects Med.* 24 (2003) 27–37.
- [25] H. Zreiqat, C.R. Howlett, A. Zannettion, P. Evans, G. Schulze-Tanzil, C. Knabe, Mechanisms of magnesium-stimulated adhesion of osteoblastic cells to commonly used orthopaedic implants, *J. Biomed. Mater. Res.* 62 (2002) 175–184.
- [26] J. Nagels, M. Stokdijk, P.M. Rozing, Stress shielding and bone resorption in shoulder arthroplasty, *J. Shoulder Elbow Surg.* 12 (2003) 35–39.
- [27] T.V. Thamaraiselvi, S. Rajeswari, Biological evaluation of bioceramic materials—a review, *Trends Biomater. Artif. Organs* 18 (2004) 9–17.
- [28] G.-L. Song, Z. Xu, Effect of microstructure evolution on corrosion of different crystal surfaces of AZ31 Mg alloy in a chloride containing solution, *Corros. Sci.* 54 (2012) 97–105.
- [29] G.-L. Song, R. Mishra, Z. Xu, Crystallographic orientation and electrochemical activity of AZ31 Mg alloy, *Electrochim. Commun.* 12 (2010) 1009–1012.
- [30] G.-L. Song, Z. Xu, The surface, microstructure and corrosion of magnesium alloy AZ31 sheet, *Electrochim. Acta* 55 (2010) 4148–4161.
- [31] G.-L. Song, Electroless" deposition of pre-film of electrophoresis coating and its corrosion resistance on a Mg alloy, *Electrochim. Acta* 55 (2010) 2258–2268.
- [32] G.-L. Song, Potential and current distributions of one-dimensional galvanic corrosion systems, *Corros. Sci.* 52 (2010) 455–480.
- [33] G.-L. Song, Effect of tin modification on corrosion of AM70 magnesium alloy, *Corros. Sci.* 51 (2009) 2063–2070.
- [34] V. Kaesel, P.-T. Tai, Fr.-W. Bach, H. Haferkamp, F. Witte, H. Windhagen, Approach to control the corrosion of magnesium by alloying, in: K.U. Kainer (Ed.), *Proceedings of the Sixth International Conference Magnesium Alloys and their Applications*, 2003, pp. 534–539.
- [35] G. Song, Recent progress in corrosion and protection of magnesium alloys—an overview of CAST's Research work, *Adv. Eng. Mater.* 7 (2005) 563.
- [36] A. Meyer-Lindenberg, H. Windhagen, F. Witte, US200410241036, "Medical implant for the human or animal body".
- [37] G. Song, Shizhe Song, Corrosion behaviour of pure magnesium in a simulated body fluid, *Acta Phys. Chim. Sin.* 22 (10) (2006) 1222–1226.
- [38] G. Song, Control of degradation of biocompatible magnesium in a pseudo-physiological environment by a ceramic like anodized coating, *Adv. Mater. Res.* 29–30 (2007) 95–98.
- [39] M.P. Staiger, A.M. Pietak, J. Huadmai, G. Dias, Magnesium and its alloys as orthopaedic biomaterials: a review, *Biomaterials* 27 (2006) 1728–1734.
- [40] A. Eliezer, F. Witte, The role of biological environments on magnesium alloys as biomaterials, in: K.U. Kainer (Ed.), *Magnesium*, Proceeding Seventh International Conference on Magnesium Alloys and their Applications, Wiley-VCH, Weinheim, 2007, pp. 822–827.
- [41] J. Levesque, D. Dube, M. Fiset, D. Mantovani, Investigation of corrosion behaviour of magnesium alloy AM60-F under pseudo-physiological conditions, *Mater. Sci. Forum* 426–432 (2003) 521–526.
- [42] G. Song, S. Song, Corrosion behaviour of pure magnesium in a simulated body fluid, *Acta Phys. Chim. Sin.* 22 (2006) 1222.
- [43] F. Witte, V. Kaesel, H. Haferkamp, E. Switzer, A. Meyer-Lindenberg, C.J. Wirth, H. Windhagen, In-vivo corrosion of four magnesium alloys and the associated bone response, *Biomaterials* 26 (2005) 3557–3563.
- [44] G. Song, Control of biodegradation of biocompatible magnesium alloys, *Corros. Sci.* 49 (2007) 1696–1701.
- [45] G. Song, S. Song, A possible biodegradable magnesium implant material, *Adv. Eng. Mater.* 9 (2007) 298–302.
- [46] L. Chang, L. Tian, W. Liu, X. Duan, Formation of dicalcium phosphate dehydrate on magnesium alloy by micro-arc oxidation coupled with hydrothermal treatment, *Corros. Sci.* 72 (2013) 118–124.
- [47] M. Tomozawa, S. Hiromoto, Growth mechanism of hydroxyapatite-coatings formed on pure magnesium and corrosion behaviour of the coated magnesium, *Appl. Surf. Sci.* 257 (2011) 8253–8257.
- [48] M. Kang, H. Jung, S. Kim, S. Lee, H. Kim, Y. Estrin, Y. Koh, Production and bio-corrosion resistance of porous magnesium with hydroxyapatite coating for biomedical applications, *Mater. Lett.* 108 (2013) 122–124.
- [49] M. Bornapour, N. Muja, D. Shum-Tim, M. Cerruti, M. Pekguleryuz, Biocompatibility and biodegradability of Mg-Sr alloys: the formation of Sr-substituted hydroxyapatite, *Acta Biomater.* 9 (2013) 5319–5330.

- [50] H. Wong, K. Yeung, K. Lam, V. Tam, P. Chu, K. Luk, K. Cheung, A biodegradable polymer-based coating to control the performance of magnesium alloy orthopaedic implants, *Biomaterials* 31 (2010) 2084–2096.
- [51] L. Xu, F. Pan, G. Yu, L. Yang, E. Zhang, K. Yang, In vitro and in vivo evaluation of the surface bioactivity of a calcium phosphate coated magnesium alloy, *Biomaterials* 30 (2009) 1512–1523.
- [52] Y. Zhao, G. Wu, J. Jiang, H. Wong, K. Yeung, P. Chu, Improved corrosion resistance and cytocompatibility of magnesium alloy by two-stage cooling in thermal treatment, *Corros. Sci.* 59 (2012) 360–365.
- [53] N. Abidin, A. Atrens, D. Martin, A. Atrens, Corrosion of high purity Mg, Mg2Zn0.2Mn, ZE41 and AZ91 in Hank's solution, *Corros. Sci.* 53 (2011) 3542–3556.
- [54] F. Witte, J. Fischer, J. Nellesen, C. Vogt, J. Vogt, T. Donath, F. Beckmann, In vivo corrosion and corrosion protection of magnesium alloy LAE442, *Acta Biomater.* 6 (2010) 1792–1799.
- [55] D. Vojtech, J. Kubasek, J. Serak, P. Novak, Mechanical and corrosion properties of newly developed biodegradable Zn-based alloys for bone fixation, *Acta Biomater.* 7 (2011) 3515–3522.
- [56] Y. Xin, K. Hou, H. Tao, G. Tang, P. Chu, Influence of aggressive ions on the degradation behavior of biomedical magnesium alloy in physiological environment, *Acta Biomater.* 4 (2008) 2008–2015.
- [57] A. Yamamoto, S. Hiromoto, Effect of inorganic salts, amino acids and proteins on the degradation of pure magnesium in vitro, *Mater. Sci. Eng., C* 29 (2009) 1550–1568.
- [58] R. Rittig, S. Virtanen, Composition of corrosion layers on a magnesium rare-earth alloy in simulated body fluids, *J. Biomed. Mater. Res. Part A* 88 (2) (2009) A359–A369.
- [59] L. Muller, F.A. Muller, Preparation of SBF with different HCO_3^- content and its influence on the composition of biomimetic apatites, *Acta Biomater.* 2 (2006) 181–189.
- [60] T. Kokubo, H. Takadama, How useful is SBF in predicting in vivo bone bioactivity, *Biomaterials* 27 (2006) 2907–2915.
- [61] Y. Xin, T. Hu, P. Chu, Degradation behaviour of pure magnesium in simulated body fluids with different concentrations of HCO_3^- , *Corros. Sci.* 53 (2011) 1522–1528.
- [62] G.-L. Song, M. Liu, The effect of surface pretreatment on the corrosion performance of electroless E-coating coated AZ31, *Corros. Sci.* 62 (2012) 61–72.
- [63] G. Song, A. Atrens, X. Wu, B. Zhang, Corrosion behaviour of AZ21, AZ501 and AZ91 in sodium chloride, *Corros. Sci.* 40 (10) (1998) 1769–1791.
- [64] W. Neuman, M. Neuman, The chemical dynamics of bone mineral, IL: University of Chicago, J. Bone Joint Surg. (1958) 34.
- [65] H. Kuwahara, Y. Al-Abdullah, N. Mazaki, S. Tsutsumi, T. Aizawa, precipitation of magnesium apatite on pure magnesium surface during immersion in Hank's solution, *Mater. Trans.* 42 (7) (2001) 1317–1321.
- [66] L. Li, J. Gao, Y. Wang, Evaluation of cyto-toxicity and corrosion behaviour of alkali-heat-treated magnesium in simulated body fluid", *Surf. Coat. Technol.* 185 (2004) 92–98.
- [67] R. Rettig, S. Virtanen, Composition of corrosion layers on a magnesium rare-earth alloy in simulated body fluids, *J. Biomed. Mater. Res. Part A* 88 (2) (2009) A359–A369.
- [68] Q. Peng, Y. Huang, L. Zhou, N. Hort, K. Kainer, Preparation and properties of high purity Mg–Y biomaterials, *Biomaterials* 31 (2010) 398–403.
- [69] A. Yamamoto, S. Hiromoto, Effect of inorganic salts, amino acids and proteins on the degradation of pure magnesium in vitro, *Mater. Sci. Eng., C* 29 (2009) 1559–1568.
- [70] W. Hynes (Ed.), CRC Handbook of Chemistry and Physics, 94th ed., 2013–2014, pp. 4.43–5.93.
- [71] G. Song, A. Atrens, D. Stjohn, J. Nairn, Y. Li, The electrochemical corrosion of pure magnesium in 1 N NaCl, *Corros. Sci.* 39 (5) (1997) 855–875.
- [72] G. Song, David Stjohn, Corrosion behaviour of magnesium in ethylene glycol, *Corros. Sci.* 46 (2004) 1381–1399.
- [73] G.-L. Song, Minghong Liu, The effect of Mg alloy substrate on "electroless" E-coating performance, *Corros. Sci.* 53 (2011) 3500–3508.
- [74] G.-L. Song, Z. Xu, Crystal orientation and electrochemical corrosion of polycrystalline Mg, *Corros. Sci.* 63 (2012) 100–112.